Bull. Chem. Soc. Jpn., 71, 1—15 (1998)

Accounts

Matrix-Isolation Spectroscopy Using Solid Parahydrogen as the Matrix: Application to High-Resolution Spectroscopy, Photochemistry, and Cryochemistry

Takamasa Momose and Tadamasa Shida*

Department of Chemistry, Graduate School of Science, Kyoto University, Kyoto 606-01

(Received September 4, 1997)

Solid parahydrogen is an excellent matrix for matrix-isolation spectroscopy. First, spectroscopic resolution exceeds the resolution attainable in conventional matrices so that detailed analysis of rotational structure of molecules in the solid phase may be performed in favorable cases. Secondly, in situ photolysis is feasible on account of the subduction of the cage effect in solid parahydrogen, which is in sharp contrast to the system in rare gas matrices. In this Account we describe 1) relevant properties of solid parahydrogen in connection with its use as the matrix, 2) outlines of experimental procedures using solid parahydrogen as the matrix, 3) examples of high-resolution spectroscopic studies, and 4) examples of studies on photochemistry and cryochemistry.

In 1954 three papers appeared independently which were concerned with techniques to stabilize reactive chemical species.[1—3] Pimentel and his co-workers utilized xenon and several polyatomic molecules to trap reactive molecules at cryogenic temperatures for spectroscopic observation.[1]Norman and Porter[2] revived the classic work of organic molecular matrices by Lewis in the early 1940's,[4] while Broida and Pellam demonstrated that reactive atoms and radicals could be stabilized by rapid cooling to liquid helium temperature.[3] All these techniques are classified as what is called today the matrix-isolation method. Since then, matrix-isolation spectroscopy has grown to be methodology for a variety of applications. Applied to the study of unstable molecules, it has piloted gas-phase spectroscopy as exemplified by the compilation of spectral data by Jacox.[5] Not only unstable but also stable molecules are the subject of studies for understanding the physics and chemistry in the condensed phase.[6]

Rare gas atoms are used predominantly as the matrix because of their chemical inertness and simplicity of physical properties, as compared with molecular matrices. However, due to homogeneous and inhomogeneous line broadening, the resolution of matrix-isolation spectroscopy is inherently limited and until recently it was considered that high-resolution spectroscopy comparable to that in the gas phase was not practicable.

In 1989, however, an eye-opening breakthrough was achieved by Okumura, Chan, and Oka. They discovered the linewidth of the $J=6\leftarrow0$ transition of solid parahydrogen was as narrow as 180 MHz (=0.006 cm^{-1} at FWHM).[7] This work was followed by the finding that the linewidth of the stimulated Raman transition of solid parahydrogen[8] and the linewidth of the rotation-vibration transition of deuterated hydrogen in solid parahydrogen[9] are even narrower, exceeding the Doppler-limited linewidth of transitions in the gas phase by one order of magnitude.[10]

We have started the research on the application of solid parahydrogen to matrix-isolation spectroscopy of polyatomic molecules. As the first step of our research the high-resolution rotation-vibration spectroscopy of methane was undertaken as a prototype of polyatomic molecules.[11—13] As a result the spectral linewidth was found to be sharp enough to resolve the fine splitting due to the intermolecular interaction between methane and hydrogen molecules. The quantitative analysis of the spectrum was possible for this ideal system.

The primary aim of one of the authors is the application of parahydrogen matrix for the study of unstable molecules such as radicals and ions which have been studied mainly by electronic absorption and ESR spectroscopy with the use of unique molecular matrices.[14—18] In this respect it was luck to find that products of in situ photolysis can be observed in hydrogen matrix as has been demonstrated by ESR spectroscopy by Miyazaki et al.[19] This is a great advantage because in the rare gas matrix the cage effect prevents effective photolysis such that if one wants to study reactive species they must be produced by pyrolysis, discharge, fast-atom-bombardment, photoexcitation, etc., prior to the deposition of solidified samples in matrices which leads to the compli-

cation of the system to be studied. The two advantages, i.e., feasibility of high-resolution spectroscopy and applicability of in situ photolytic technique, should hopefully pave a new avenue for matrix-isolation spectroscopy of both stable and unstable molecules.

Hydrogen matrix is being studied from a somewhat different angle also; Fajardo et al. are exploring spectroscopy in the visible to VUV region and reactive dynamics of dopants in the matrix with the ultimate purpose of finding high-performance rocket propellants.[20] The study is descended from a national project exploring free radical rockets.[21]

Oka described his article on spectroscopy of solid hydrogen as a "glaringly premature review".[10] The present article is even more so. Nevertheless, anticipating the viability of the method of parahydrogen matrix, we will present not only our recent work but also some background information on solid parahydrogen for general understanding of the new matrix.

Physical Properties of Solid Parahydrogen

The nuclear spin state of diatomic hydrogen is symmetric and antisymmetric with the statistical weights of three and one, respectively. The former and the latter are associated with the rotational states of odd and even quantum numbers, respectively, and are conventionally called ortho and parahydrogen. Since the conversion between the two classes of nuclear spin state is slow in the absence of magnetic perturbation, ortho and parahydrogen behave like different molecules in the practical time scale. At room temperature hydrogen gas consists of ortho and parahydrogen in a ratio of three to one, which is called normal hydrogen.

Being the smallest mass molecule, the rotational constant of hydrogen is as large as 60.853 cm^{-1} and the energy gap between the first excited ($J=2$) and the ground ($J=0$) rotational states of parahydrogen is 354.38 cm^{-1}. The corresponding gap between the states of $J=3$ and 1 for orthohydrogen is even larger at 587.06 cm^{-1}.[22] Therefore, at liquid helium temperatures in the present work practically all para and orthohydrogen molecules are in the rotational states of $J=0$ and 1, respectively. Hereafter, the terms of para and orthohydrogen are used to signify the hydrogen molecule with $J=0$ and 1, respectively.

On account of the spherical symmetry of the rotational wavefunction of parahydrogen the expectation value of all averaged permanent multipole moments of parahydrogen is zero, whereas orthohydrogen has a permanent quadrupole moment of the lowest order multipole moment. Thus, although parahydrogen is a diatomic molecule, its electrostatic character is spherical as in rare gas atoms.

Only the weak dispersion force assembles the parahydrogen molecules into a van der Waals crystal. The crystal has a hexagonal close packed (hcp) structure belonging to point group of D_{3h}. Figure 1 shows the crystal structure where the crystal axes a and b are in the hexagonal plane denoted by α or β and the axis c is perpendicular to the planes. Of the twelve nearest neighbor molecules, six are in the hexagonal plane and the rest are above and below the plane. The unit

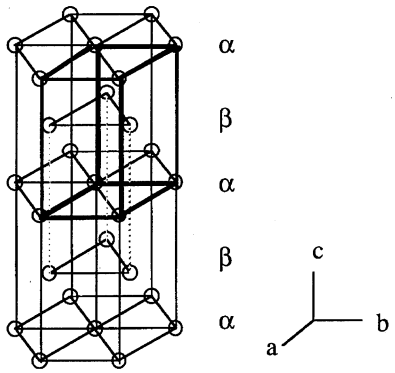

Fig. 1. Hexagonal close packed structure of solid hydrogen.

cell contains two molecules with the middle point being the center of inversion.

A remarkable feature of this crystal is that the nearest neighbor distance, i.e., lattice constant, is 3.783 Å and the zero-point lattice vibrational amplitude is as large as approximately 18% of the lattice constant.[23] Such a large zero-point motion defies treatment by the classical theory of lattice dynamics. For this reason, solid parahydrogen is called a quantum solid, along with the solids of ^{3}He and ^{4}He.[24] A short discussion following Silvera[23] on such solids may be helpful: The ground state of a solid is determined, given the Hamiltonian

$$H=-\frac{1}{2}\lambda^2\sum_i\nabla_i^2+\frac{1}{2}\sum_{i\neq j}v(i,j),$$

where $\lambda^2=\hbar^2/(\sigma^2 m\varepsilon)$ is called the de Boer quantum parameter; it is a measure of the relative contributions of kinetic versus potential energies approximated by a sum over all pair-wise interactions. The parameters σ and ε are the core radius and the potential well depth appearing in the Lennard–Jones 6—12 pair potential, which is proportional to $\varepsilon[(\sigma/r)^{12}-(\sigma/r)^6]$. The parameter λ is used to reduce the Hamiltonian to a dimensionless form. The lighter the particle and the shallower the potential (smaller ε), the larger is λ. As specific examples, we have, $\lambda^2(H_2)=0.076$, $\lambda^2(Ne)=0.0049$, and $\lambda^2(Ar)=0.0027$.

The large contribution of kinetic energy of zero-point vibration in the hydrogen crystal causes repulsions between hydrogen molecules in the crystal to result in the large lattice constant of 3.783 Å which is approximately 10 to 20% larger than the distance in the H_2–H_2 van der Waals cluster. A measure of the localization of the particles to their equilibrium positions in a crystal is given by the ratio of the root-mean-square (rms) amplitude relative to the lattice constant.[23] The rms amplitudes are shown to be a linear function of λ and are given as 0.18, 0.09, and 0.05 for H_2, Ne, and Ar at 0 Kelvin, respectively.[25] Thus, while in solid Ar, the atoms are nearly localized to the lattice site, the zero-point vibrational amplitude of solid H_2 amounts to 18% of the lattice constant. Therefore, solid parahydrogen may be considered a spacious and "soft" medium compared with ordinary rigid, non-quantum solids such as rare gases.

In addition to the above structural feature, the energy

density of solid parahydrogen is exceptionally sparse for a molecular solid because the rotational constant of 60.853 cm^{-1}, the fundamental vibrational frequency of 4401.2 cm^{-1}, and the first excited electronic energy of 91700 cm^{-1} all exceed the corresponding parameters of other molecules. Furthermore, the Debye temperature, which characterizes the lattice motion in terms of temperature, amounts to approximately 100 K($\cong$70 cm^{-1}).[23,25] All these features imply that the relaxation of excited molecules in solid parahydrogen is extraordinarily slow, which means, in turn, that the solid can be a superb medium for high-resolution matrix isolation spectroscopy.

Experimental Procedures

Ortho–Para Conversion. As stated above, all averaged permanent multipole moments of parahydrogen are zero, while orthohydrogen has a quadrupole moment of the lowest multipole moment. The existence of orthohydrogen in solid parahydrogen causes inhomogeneity of the internal electrostatic field which leads to spectral line broadening in spectroscopic measurements when solid parahydrogen is used as a matrix. Therefore, for spectroscopic applications the concentration of orthohydrogen should be reduced as much as possible. At thermal equilibrium, the concentration of orthohydrogen is 75% at room temperature, approximately 0.4% at the boiling point of liquid hydrogen (20.28 K at 1 atm), and approximately 0.0045% at the triple point (13.80 K). Therefore, the conversion should be carried out at temperatures as low as possible. With the ortho–para converter used in these experiments (Fig. 2), it is possible to obtain parahydrogen contaminated with orthohydrogen at approximately 0.01% or less. The catalyst is commercial iron (III) hydroxide.

Sample Preparation. Solid parahydrogen is a good heat conductor as a quantum solid (see the section "Comment on Cage Effect"). Therefore, the growth of the hcp crystal proceeds with ease compared with other substances used as the matrix. In most of our experiments, gaseous parahydrogen containing a small amount of the foreign molecules under investigation is introduced through a thin stainless steel tubing to a copper cell. This sample chamber has an inner diameter of 2 cm and a length of 10 cm, with appropriate optical windows at both ends attached with indium gaskets. The mixed gas starts to solidify uniformly onto the copper surface and the crystal grows toward the center of the cylindrical copper cell. The appearance of the solidified sample is visually transparent. Optical measurements using polarized light indicate that the crystalline c axis grows in the radial direction. The transparent solid sample with a long path of 10 cm is advantageous in the optical experiment. For a sample containing 0.001% foreign molecules in solid parahydrogen, whose molar volume is 23.06 cm^3 mol^{-1},[23,25] the column density of the foreign molecule in such a cell amounts to 2.6×10^{18} molecules cm^{-2}. The density corresponds to a gaseous sample with a pressure of 100 mTorr (1 Torr=133.322 Pa) and an optical path length of 750 m.

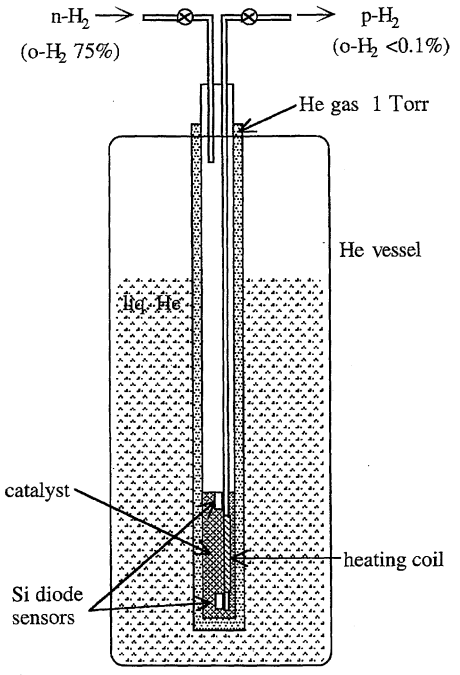

Fig. 2. Ortho–para converter. *n*-Hydrogen is cooled down to liquid hydrogen and is forced to percolate through an iron(III) hydroxide catalysis.

The concentration of foreign molecule in the premixed gas ranges typically from 0.005 to 0.02%. The proper choice of the concentration is crucial to control the degree of isolation of the foreign molecule. In order to obtain well isolated samples the concentration in the premixed gas is made as low as possible while for cluster-rich samples higher concentrations are chosen.

As for mixing nonvolatile samples, a small amount of a solid sample is placed in the optical cell and laser-vaporized with a Q-switched Nd : YLF laser delivering a pulse of 200 μJ per pulse with a repetition rate of 200 Hz. During the vaporization, parahydrogen gas is introduced into the optical cell.

The temperature of the cell is kept at 7 to 8 K during the deposition and is lowered to approximately 5 K for the optical measurement. Since the change of density of solid parahydrogen is little at temperatures below approximately 7 K, sudden shrinkage of the solid leading to mechanical cracks can be avoided by preparing the crystal around 7 K. The temperature of the sample deposition is also important to control the degree of isolation; lower temperatures give better isolation while higher temperatures tend to yield cluster-rich samples.

Optical Measurement. Due to the wide range of the optical transparency of solid parahydrogen, various optical measurements extending from VUV to far-IR are feasible. For IR spectroscopy, a commercial Fourier transform infrared (FTIR) spectrometer was used for quick survey, while CW IR laser systems were used for high-resolution spectroscopy.

The linewidth of transitions in solid parahydrogen is seen in the order of 0.0001 cm^{-1} for the stimulated Raman pure vibrational transition of solid parahydrogen.[8] Therefore, a laser light source of spectral purity of 0.0001 cm^{-1} is desired for high-resolution spectroscopy. CW lasers are indispensable because pulse lasers with a pulse duration shorter than 1 nano sec are incapable of attaining such spectral purity due to the uncertainty principle. Depending on the frequency region, difference-frequency lasers, color center lasers, diode lasers and so on, are employed. In our experiment, difference-frequency lasers are used to cover the frequency range of 900 to 9000 cm^{-1}. A typical set-up is shown in Fig. 3.[26]

The signal is detected by semiconducting detectors. Since the sample is in the solid state, molecular modulation such as velocity modulations familiar in gas phase spectroscopy is not applicable. Instead, high-sensitivity and high-resolution detection are attained by tone-burst frequency modulation technique.[27] In this technique, frequency side bands produced by mixing laser radiation with a

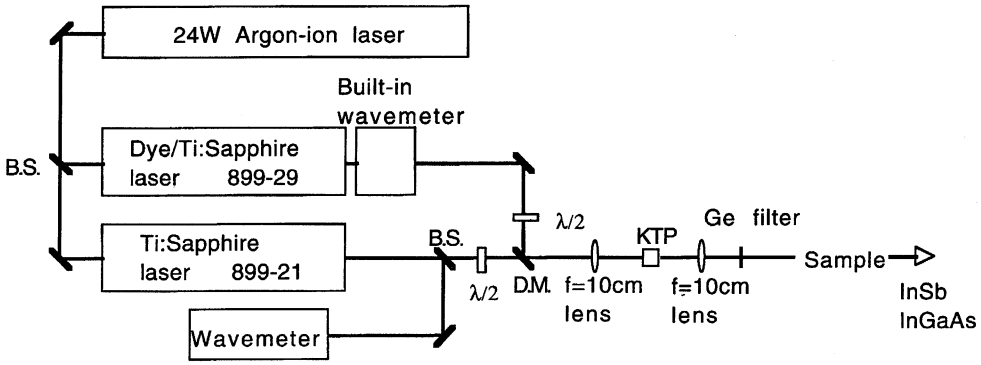

Fig. 3. Difference-frequency laser system.

radio frequency from several MHz up to several hundreds MHz in a nonlinear crystal are on and off; then the signal is demodulated by a usual phase-sensitive-detector. By this technique, a signal change down to approximately 5×10^{-5} is detectable.

High-Resolution Spectroscopic Application

Methane. The molecular rotation in condensed phase was first discussed by Pauling back in 1930.[28] The rotational motion of methane was experimentally studied in rare gas matrices as well as in solid nitrogen.[29—34] The observed vibrational spectra exhibit multiplets which are regarded as partial revelation of rotational structure. However, in these conventional matrices multiple trapping sites tend to occur which give spectral signals at slightly different frequencies. Moreover, the rotation of methane is partially prevented by the rigid matrix. Therefore, complete analysis of the observed spectra in these matrices has not been reported.

In solid parahydrogen, methane may be trapped in an almost free space because removal of one hydrogen molecule from the crystal produces a void of a diameter of approximately 7.6 Å (Fig. 1) which is ample enough to accommodate a methane molecule with a van der Waals radius of about 1.62 Å. Moreover, since the parahydrogen crystal is a quantum solid, mechanical strain causing multiple trapping sites in non-quantum solids may be absent in the crystal. Thus, methane in solid parahydrogen allows quantitative analysis of the rotation-vibration spectrum. The FTIR spectra of 0.001% methane in solid parahydrogen at 4.8 K (Fig. 4) indicate that both the triply degenerate stretching (ν_3) and bending (ν_4) vibrational transitions accompany multiplet structures with a spacing of approximately twice the rotational constant of methane. It is instructional to discuss the spectra in some detail.

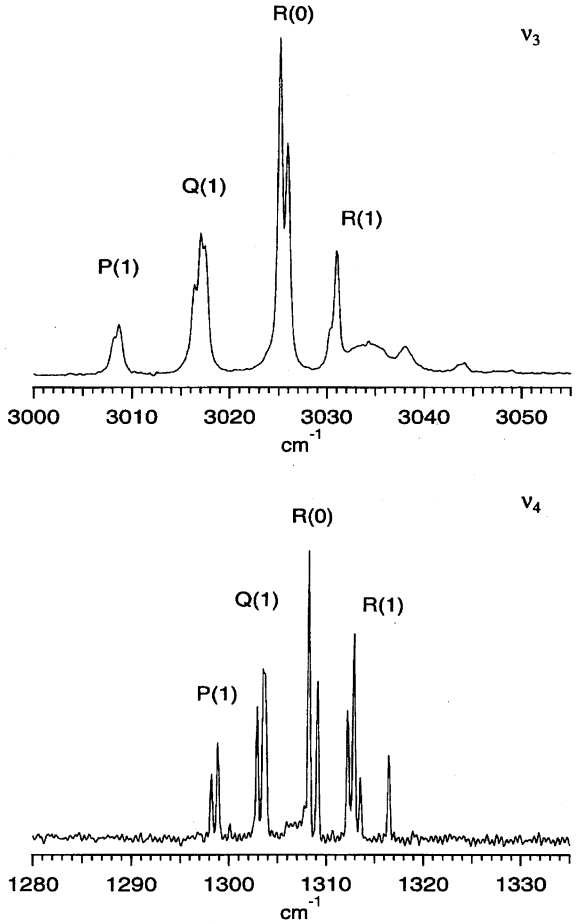

Fig. 4. FTIR spectra of ν_3 and ν_4 modes of methane observed in solid parahydrogen.

Since the rotational constant of methane in free space is 5.24 cm^{-1}, the population of $J=0$ and 1 of methane in solid parahydrogen at 4.8 K would be approximately 90 and 10%, respectively, according to the Boltzmann distribution neglecting the nuclear spin modification. Such a distribution is not realized, however, because there are three nuclear spin states with $I=2$, 1, and 0, and the conversion among them is very slow. The three states are labelled, respectively, A, F, and E according to the permutation-inversion group theoretical representation. Since the total wavefunction should be antisymmetric with respect to the exchange of identical protons, combinations of nuclear spin and rotational states are restricted, accordingly. For the electronic and vibrational ground state, the rotational state of $J=0$ is associated with the nuclear spin state of $I=2$ (A-state), while the state of $J=1$ couples with the state of $I=1$ (F-state). As for the rotational state of $J=2$, both the states of $I=0$ (E-state) and $I=1$ (F-state) are possible. In our experiment the mixed gas of methane and parahydrogen is cooled from room temperatures to cryogenic temperatures much faster than the rate of the nuclear

spin state conversion of methane, leaving the population ratio of A, F, and E states of methane in solid parahydrogen in almost the same ratio as at room temperature, i.e., 5 : 9 : 2.[35] Thus, even at cryogenic temperatures the rotational states of J=0, 1, and 2, associated with the different nuclear spin states A, F, and E, are initially populated roughly in the above ratio.

Parahydrogen is inevitably contaminated by residual orthohydrogen which has a magnetic dipole moment (see the section "Ortho–Para Conversion"). Due to this dipole moment the nuclear spin state conversion is accelerated and the population ratio of J=0, 1, and 2 slowly approaches the Boltzmann distribution ratio of $1(J=0):0.1(J=1):0.001(J=2)$ at 5 K. This is evident from the two upper spectra in the left and right columns of Fig. 5 where the multiplets of the ν_3 and ν_4 transitions show a temporal change in the intensity distribution among the multiplets.

Since the components of the multiplets other than the central one almost disappear after 48 h, the disappearing components are assigned to J=1 and/or 2, whereas the central one is assigned to J=0. Referring to the gas phase rotational constant the multiplets are identified as designated in Figs. 4 and 5. The missing of J=2 rotational state is tentatively accounted for as follows: in the rotational state of J=2, both E (I=0) and F (I=1) nuclear spin states are allowed, as mentioned above. Therefore, in this rotational state the nuclear spin states E and F can mix, and the rotational state of J=2 coupled with E may relax to J=1 via the E–F mixing within the experimental time scale.

It is now possible to analyze the fine structure superimposed on each component of multiplets; this is seen in Figs. 4 and 5. Fine structure is due to crystal field splitting of the M degeneracy in the rotational wavefunction of methane, where M is the projection of the rotational quantum number J along the space-fixed axis. The analysis leads to the energy diagram (Fig. 6) for methane in solid parahydrogen, as compared with the diagram in the gas phase.

Since both the ν_3 and ν_4 transitions are triply degenerate,

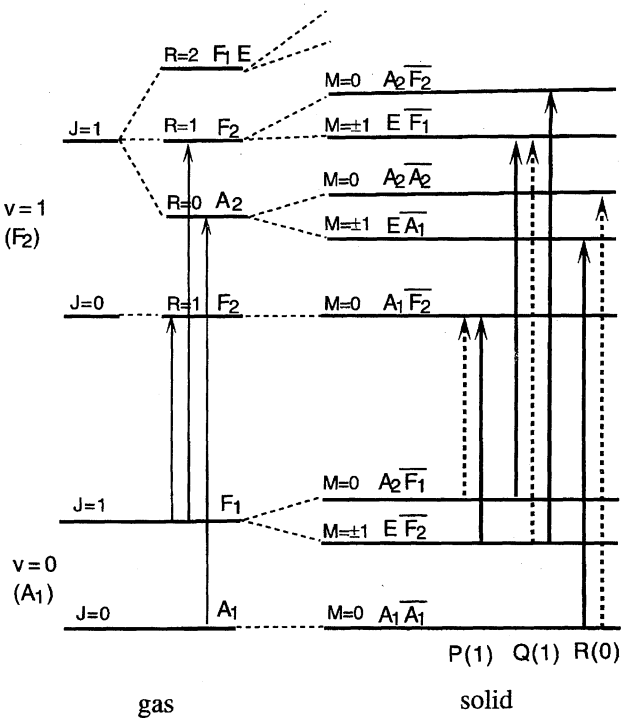

Fig. 6. Energy diagram of methane in gas (left) and in solid parahydrogen (right) applicable both to ν_3 and ν_4 modes. The scale of the energy is arbitrary.

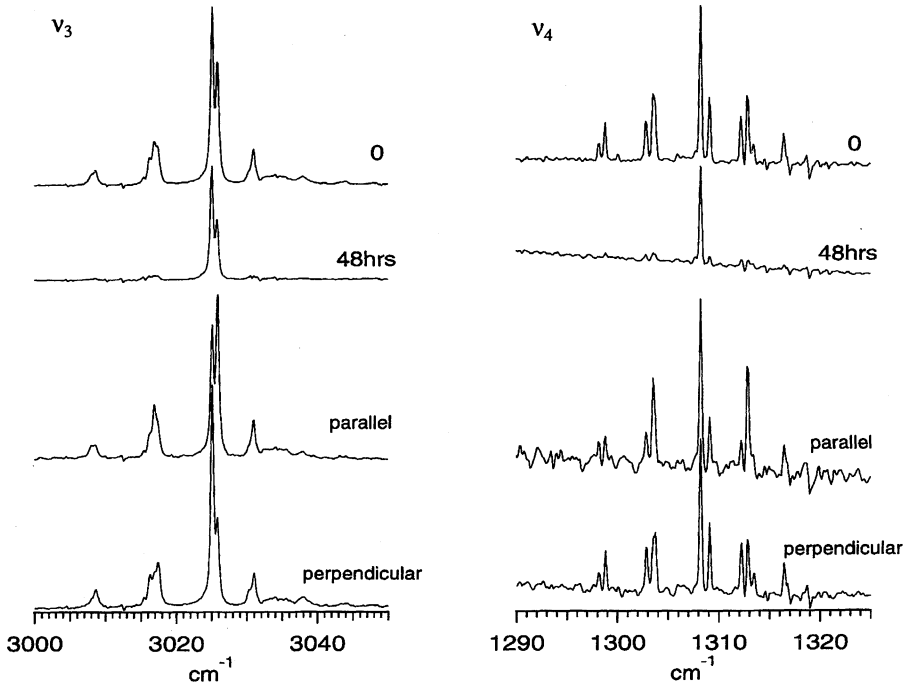

Fig. 5. Temporal changes of the absorption of ν_3 and ν_4 modes of methane (upper two panels) and the polarization dependence (lower two panels).

the rotation-vibration state in the gas phase is split by the Coriolis interaction. Each rotation–vibration state is labelled with a quantum number $R=J+l$, where l stands for the vibrational angular momentum. The energy levels shown to the left of Fig. 6 illustrate the gas-phase levels designated by the symmetry representation of point group T_d.

For the analysis of methane in solid parahydrogen, an approach based on an extended group theory developed by Miller and Decius is employed.[36] This approach considers the product group G='S'×'$\overline{\text{M}}$', where S and $\overline{\text{M}}$ stand for the groups to which the crystal and the molecule of concern (methane) belong. The product group is not the direct product in the usual sense, but it is an ensemble of products of elements of S and $\overline{\text{M}}$, with each pair of elements possessing a common parity. The symbol ' ' signifies that G is composed of only the elements satisfying this parity restriction. In the particular case of methane in solid parahydrogen, S belongs to point group D_{3h} consisting of the elements $\{E, 2C_3, 3C_2, \sigma_h, 2S_3, 3\sigma_v\}$ while $\overline{\text{M}}$ is the permutation-inversion group isomorphic to T_d and consists of the elements $\{E, 8(123), 3(14)(23), 6(1423)^*, 6(23)^*\}$. Here, the symbols such as (123) represent permutation operation of hydrogen nuclei and the asterisk stands for the space inversion operation. Selecting only the elements sharing the same parity from S and $\overline{\text{M}}$, we obtain G as follows, $\{E\overline{E}, 8E\overline{(123)}, 3E\overline{(14)(23)}, 6\sigma_h\overline{(1423)^*}, 6\sigma_h\overline{(23)^*}, 2C_3\overline{E}, 16C_3\overline{(123)}, 6C_3\overline{(14)(23)}, 12S_3\overline{(1423)^*}, 12S_3\overline{(23)^*}, 3C_2\overline{E}, 24C_2\overline{(123)}, 9C_2\overline{(14)(23)}, 18\sigma_v\overline{(1423)^*}, 18\sigma_v\overline{(23)^*}\}$. In the above, the bar emphasizes the operation is to be applied to a molecule. The group G may be written as the direct product of D_3, a subgroup of D_{3h}, and T_d as $G=D_3\times\overline{T}_d$ whose character table is equivalent to the direct product of the character tables of D_3 and T_d.[11]

With this in mind, it is possible to proceed to label the rotational state of methane in the parahydrogen crystal. First, the rotational wavefunction of methane $|JKM>$ is expressed in terms of Wigner's rotation matrix as $|JKM>=\sqrt{(2J+1)/(8\pi^2)}D^J_{KM}(\chi\theta\phi)$. Note that the effect of the operation of the elements of group G upon the wavefunction can be expanded as follows.

$$R_{\alpha\beta\gamma}\overline{R}_{\alpha'\beta'\gamma'}|JKM> = \sum_{K'M'} D^J_{M'M}(\alpha\beta\gamma)D^J_{KK'}(\alpha'\beta'\gamma')|J'K'M'>.$$

In the above equation the sets of angles $\alpha\beta\gamma$ and $\alpha'\beta'\gamma'$ represent the symmetry operations of the space and the molecular groups expressed in terms of the Euler angles.[37] Finally, referring to the character table of G and using the so-called generating machine technique of Van Vleck,[38] the desired labelling is accomplished. For example, in the vibrational ground state it is found that $|J=0, M=0>$ belongs to $A_1\overline{A_1}$ while $|J=1, M=0>$ belongs to $A_2\overline{F}_1$.[11]

In order to derive the optical selection rule, it is necessary to know the symmetry of the space fixed dipole moment, which is found from the character table as $\mu_z\leftrightarrow A_2\overline{A_2}$ and $\mu_x, \mu_y\leftrightarrow E\overline{A_1}$. The above symmetries are equivalent to the products of the symmetries of the dipole moment in the subgroup D_3 of the crystal group D_{3h}, i.e., $A_2(\mu_z)$ and $E(\mu_x, \mu_y)$, multiplied by the totally symmetric $\overline{A_1}$ or the antisymmetric $\overline{A_2}$ of the molecular group T_d.

In Fig. 6, all the labels derived in this way for the $J=0$ and 1 rotational states are designated. By combining these symmetry labels with those of the space-fixed dipole moments, the optically allowed transitions; these are marked by the vertical arrows, are obtained. Dotted arrows correspond to the transitions polarized parallel to the crystal c axis, whereas solid arrows represent perpendicular transitions. It is seen that the transition of P(1) in the gas phase is split into a doublet; the splitting is attributed to the removal of degeneracy in the vibrationally ground state. In contrast, the splitting in R(0) is attributed to splitting in the excited level.

The result demonstrated in Fig. 6 can be used to analyze the lower two spectra in the left and right columns of Fig. 5, where the result of polarization measurements is shown. In each column, the upper of the two spectra is obtained when the probing IR beam is polarized parallel to the crystal c axis, which is along the radial direction of the sample in the cylindrical cell, whereas in the lower spectra impinging light is perpendicular to the axis. Since the beam diameter is relatively large, polarization of the probing light is not complete. Nevertheless, the difference between the upper and the lower spectra is clear enough to allow us to determine the magnitude of the splitting and the order of energy level among the split M sublevels. For example, from the structure of P(1) the splitting in the $v=0$, $J=1$ level is obtained at 0.64 cm^{-1} and the sublevel of $M=0$ is determined to be above that of $M=\pm1$.

It is now necessary to consider the crystal field splitting in a quantitative way. If the orientation of methane in the crystal is represented by angle Ω, the crystal field potential $V(\Omega)$ must be invariant under any symmetry operation on both the molecule and the crystal, i.e., the potential must belong to the totally symmetric species $A_1\overline{A}_1$ of group G discussed above. Expressing the potential in terms of Wigner's rotation matrix, we find the lowest order anisotropic crystal field satisfying the above symmetry restriction to be[11]

$$V(\Omega)=\frac{1}{2}\varepsilon_{3c}[D^3_{2,3}(\Omega)+D^3_{2,-3}(\Omega)-D^3_{-2,3}(\Omega)-D^3_{-2,-3}(\Omega)].$$

With the use of this potential, the analysis of the observed spectra yields the crystal field parameter $\varepsilon_{3c}=-25.8$ cm^{-1} together with the rotational constants of 4.793 cm^{-1} (ground), 4.603 cm^{-1} (ν_3), 4.591 cm^{-1} (ν_4), the band origins of 3017.26 cm^{-1} (ν_3) and 1303.62 cm^{-1} (ν_4), and the Coriolis parameters of 0.0450 cm^{-1} (ν_3) and 0.4654 cm^{-1} (ν_4).[12] The rotational constants in solid parahydrogen are about 10% smaller than those in free space. The increase of the effective mass of methane in the solid due to the intermolecular interaction accounts for the decrease of the rotational constants. From the value of the crystal field parameter obtained above, the anisotropic dispersion potential between a pair of one methane and one hydrogen molecule expressed as $V_3=A_3[D^3_{2,0}(\Omega)-D^3_{-2,0}(\Omega)]/\sqrt{2}$ is determined as $A_3=34.5$ cm^{-1} at an intermolecular distance of 3.78 Å which is

taken to be equal to the lattice constant of the parahydrogen crystal.[11,12] The result demonstrates that spectral data obtained from the system in solid parahydrogen can provide quantitative information on the intermolecular interaction. Such an achievement cannot be expected for conventional rare gas matrices because of the ambiguity of spectral assignment.

In addition to this remarkable advantage, parahydrogen matrix is superior to the others in the estimation of the value of the transition frequency in free space, that is to say, the matrix-shift is smaller than that in conventional matrices. Table 1 lists the frequencies in matrices and in the gas phase for methane along with methyl radical; the latter will be discussed in the subsequent section. If the rotational constant B of the vibrationally excited state is equal to the constant of the ground state, the transition frequency of Q(1) corresponds to the band origin and the difference of R(0)−P(1) corresponds to $4B(1-\zeta)$, where ζ is the Coriolis constant.[39] In the gas phase B=5.28 cm^{-1} and ζ=0.464 for the ν_4 mode. Both the fequency of Q(1) and the difference R(0)−P(1) observed in parahydrogen matrix are closer to the gas phase values than in other matrices. The data for the ν_3 mode of methane (data not shown) also show a similar tendency. There is no report on methane in a neon matrix.

Figure 7 shows the expanded spectrum of a portion of R(0) of the ν_4 mode of methane recorded by using a difference-frequency laser system composed of two ring dye lasers and a $AgGaS_2$ non-linear crystal.[12] The apparent singlet in the FTIR measurement is shown to actually comprise of more than 20 lines with an average linewidth of approximately 0.003 cm^{-1}. Since each components varies in intensity in different directions of polarized laser light, we think that the

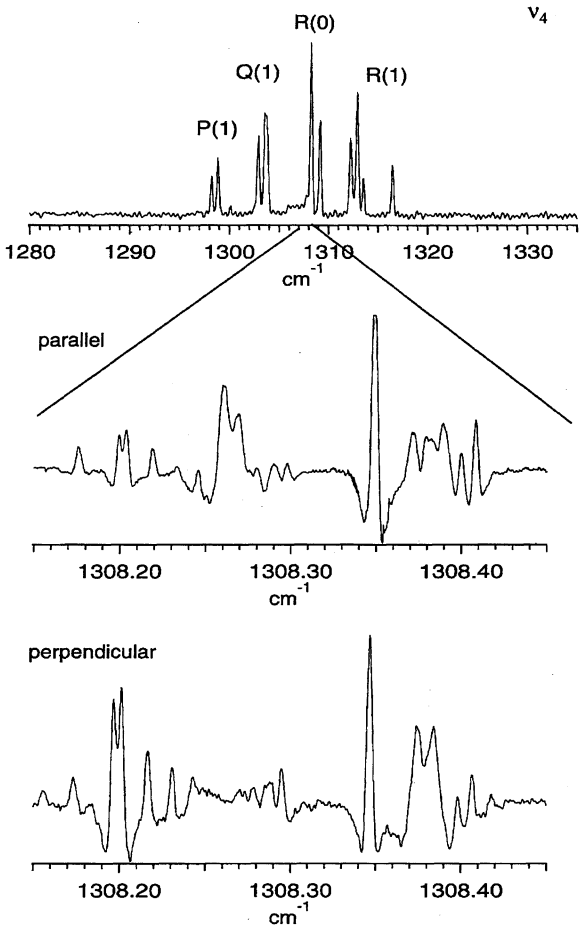

Fig. 7. High-resolution spectra of the R(0) line of ν_4 mode. Middle and bottom panels which are recorded by laser light polarized parallel and perpendicular to the crystal c axis, respectively.

Table 1. Transition Frequencies of Methane and Methyl Radical in Various Media in Units of cm^{-1}

ν_4 of CH_4[32,33]

	Q(1)	R(0)–P(1)
Xe	1295.71	9.8
Kr	1299.06	8.6
Ar	1302.38	7.9
N_2	1302.25	8.5
p-H_2	1303.59	10.0
Gas	1305.809	11.138

$^rR_0(0)$ in ν_3 and ν_4 of CH_3[43]

	ν_3	ν_4
Ar	3150	1397.5
Ne	3162	1396
p-H_2	3170.4	1401.6
	3170.6	1402.7
Gas	3174.2935	

The transition frequency of Q(1) of methane corresponds to the band origin when the rotational constant B of the vibrational excited state is assumed to be equal to B in the ground state. The difference of R(0)–P(1) of methane corresponds to $4B(1-\zeta)$, where ζ is the Coriolis constant.[41] In the gas phase, B=5.28 cm^{-1} and ζ=0.464 for the ν_4 mode.

lines are also due to intermolecular interaction. A plausible explanation is that the product state of neighboring methane and orthohydrogen, $|JKM>_{CH_4}|J=1, M>_{H_2}$, is split by the intermolecular interaction.[12]

Similarly, more than 200 peaks of a linewidth of approximately 0.007 cm^{-1} are observed when the concentration of methane is increased to favor methane clusters.[13] The spectrum is suspected to be due to a dimer of methane whose rotational state is quantized as in the case of monomeric methane.[13] Although detailed analysis of these many-line spectra is yet done, such spectral data are most precious to deduce information on intermolecular interactions, which is difficult to obtain even by gas-phase high-resolution spectroscopy.

The linewidth of the ν_3 (stretching) mode is found to be approximately 1 cm^{-1} while that of the ν_4 (bending) mode is approximately 0.003 cm^{-1}.[12] The marked difference suggests that the former is more strongly coupled with the lattice motion.[12] The analysis of the difference will provide essential information on the vibrational relaxation of molecules in solid.

Methyl Radical. As will be discussed in the section on

Photolysis of Methyl Iodide, parahydrogen matrix allows in situ photolysis of methyl iodide to give methyl radicals. Figure 8 shows FTIR spectra of the doubly degenerate stretching (ν_3) and bending (ν_4) modes along with the overtone $2\nu_4$. The two fundamentals agree with the reported spectra of the radical in the gas phase[40] and in a rare gas matrix,[41—43] while the overtone of ν_4 is detected for the first time in the present work.[44] As a prototypical organic radical, methyl radical has been analyzed in the same way as methane. To avoid redundancy the result will be described briefly.

At first, it is noted that the difference of the linewidth between ν_3 and ν_4 is similar to the case of methane. The linewidth of the latter is determined to be approximately 0.002 cm^{-1} by laser spectroscopy as shown in the inset in the mddle trace of Fig. 8. The extended group appropriate for the system is G='D_{3h}'×'$\overline{D}_{3h}$'. The symmetry species of each rotational level and the optical selection rule are obtained by considering that the symmetry of the electronic ground state of methyl radical is $^2A_2''$ and that the symmetries of the space-fixed dipole moments are $A_2\overline{A}_2''$ and $E\overline{A}_1'$. As a result, the spectra in Fig. 8 are assigned as $^rR_0(0)$ (v=1, N=1, K=1←v=0, N=0, K=0) for both ν_3 and ν_4 and the doublet is due to the removal of the M-degeneracy. Since there

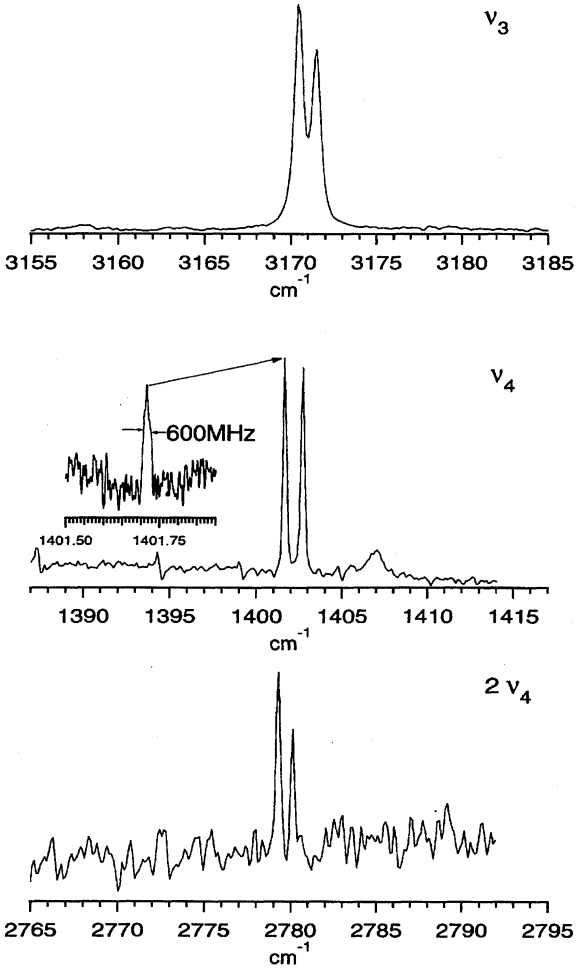

Fig. 8. FTIR spectra of ν_3, ν_4, and $2\nu_4$ modes of methyl radical observed in solid parahydrogen.

are two nuclear spin states of A and E symmetry, one may expect that not only N=0 but also N=1 are populated. The absence of the absorption associated with N=1 is understood as resulting from the near-lying paramagnetic iodine atom, which accelerates the relaxation of the excited nuclear spin state of methyl radical.

The latter half of Table 1 gives the transition frequencies of the radical in various media. As shown by Jacox,[43] the rotational level of the radical in neon and argon is considered to be quantized. Therefore, the frequency of the ν_3 transition in these matrices is compared with the frequency of $^rR_0(0)$ in the gas phase. As in the case of methane, the matrix-shift in parahydrogen matrix is remarkably small.

Carbon Clusters. As stated in the section on Sample Preparation, laser vaporization enables us to deal with solid samples. As an example, a carbon rod was ablated to obtain spectra of carbon clusters.[45] Absorptions at 2035 to 2044, 2164 to 2166, and 2007 to 2010 cm^{-1} are identified with C_3, C_5, and C_9, respectively, while an absorption at 2077 to 2080 cm^{-1} is newly detected and not yet assigned. Some of the absorptions in solid parahydrogen accompany fine structure which seems to be due not to multiple trapping sites, but to tunneling motion of the clusters.[45] Farjardo et al also reported similar spectra.[46] Such results await further investigation.

Application to Photolytic Study

A Comment on Cage Effect. Photoinduced dynamical processes such as isomerization and bond dissociation are frequently observed in polyatomic molecular matrices at liquid nitrogen temperature, as shown by Porter[2] and by the authors.[14—18] However, in rare gas matrices at cryogenic temperatures, photodissociation of a molecule is prevented by the cage effect. Exceptional cases can be grouped into the following three categories: 1) one of the products of photolysis is a stable molecule, e.g., $CF_2N_2 \rightarrow CF_2+N_2$ and $CH_2N_2 \rightarrow CH_2+N_2$; 2) two radical products are spatially intervened by the third stable molecule, e.g., $CH_3N_2CH_3 \rightarrow CH_3+N_2+CH_3$ and $C_2H_5CO\text{–}OO\text{–}COC_2H_5 \rightarrow C_2H_5 + 2CO_2 + C_2H_5$; 3) one of the photofragments is a hydrogen atom which can escape from the cage because of its small size, e.g., HI→H+I and HCN→H+CN.

Due to the cage effect, photolysis of methyl iodide, for example, cannot be investigated in rare gas matrices, in contrast to numerous studies in the gas phase. This negative conclusion is reached after several attempts by previous workers who reported "the photolysis of CH_3I in Xe did not result in CH_3",[47] "CH_3I in Ar is difficult to photolyse",[48] "in situ photolysis of CH_3I in Ar failed due to the cage effect",[49] and "the cage effect of CH_3I in Ne is near complete".[50]

However, it happens that molecules in solid parahydrogen are subjected to photolysis into radical fragments, as is shown for alkyl iodides[19,44,51,52] and carbonyl compounds.[53] We may attribute this feature to the fact that solid parahydrogen has a large lattice constant and experiences a large amplitude zero-point lattice vibration (see the section "Physical Properties of Solid Parahydrogen") which

results in a large value for the compressibility χ_T, defined as $\chi_T=-\frac{1}{V}(\partial V/\partial P)_T$ (equivalent to the inverse of bulk modulus). At temperatures below approximately 5 K, $\chi_T(p\text{-}H_2)$ is approximately 50×10^{-10} Pa^{-1},[23] which is distinctly larger than $\chi_T(Ne)\cong9\times10^{-10}$ Pa^{-1}, $\chi_T(Ar)\cong4\times10^{-10}$ Pa^{-1}, and $\chi_T(Kr)\cong3\times10^{-10}$ Pa^{-1}).[54] Solid parahydrogen at liquid helium temperature also has a large value for the thermal conductivity when the concentration of orthohydrogen is low. For a sample containing 0.2% orthohydrogen, the value for the conductivity is approximately 50 W m^{-1} K^{-1},[23] which is several times larger than the conductivity of rare gas solids.[54] The soft, compressible "wall" would allow fragments to be separated easily and the high thermal conductivity would quickly freeze out the separated fragments.

Photolysis of Methyl Iodide. Figure 9 shows FTIR spectra of approximately 0.01% methyl iodide in solid parahydrogen before (lower panel) and after UV irradiation (upper panel) at approximately 5 K. Notations I, R, M, and E stand for the methyl iodide, methyl radical, methane, and ethane, respectively, which are assigned by referring to the literature.[44] The success of the photolysis is clearly observed by the decrease of the I bands and the appearance of bands corresponding to photolysis products. Similar spectral changes are observed (data not shown) in regions where iodide absorption at 1440—1420, 1410—1395, and 1250—1235 cm^{-1} diminishes upon UV irradiation, and the absorptions of R as a doublet at 1402.7/1401.6 cm^{-1} (lower spectrum of Fig. 8) appear along with the absorption of M at 1320—1295 cm^{-1} (lower spectrum of Fig. 4).[44] UV irradiation is performed by using a 20 W mercury lamp emitting mainly 253.7 and 184.9 nm lines.[44]

The successful photolysis (Reaction 1) is contrary to the case in conventional rare gas matrices. The absorption of the radical remains unchanged after standing at 5 K for several days. Thus, the reaction between the radical and the matrix hydrogen (Reaction 2) does not proceed appreciably at cryogenic temperatures.

$$CH_3I + h\nu\ (253.7\ nm, 184.9\ nm) \rightarrow CH_3 + I, \quad (1)$$

$$CH_3 + H_2 \not\rightarrow CH_4 + H\ (at\ 5\ K). \quad (2)$$

In order to explain the appearance of methane, the wavelength dependence of the photolysis in Reaction 1 was tested by cutting the component at 184.9 nm with a filter. It was found that, with photons of 253.7 nm, only methyl radical but not methane was formed.[55] Furthermore, when this sample was continuously irradiated with photons of 184.9 nm, the radical was gradually diminished and methane was formed.[55] The test leads to the following two conclusions: 1) Since methyl radical starts to absorb at wavelengths shorter than approximately 216.4 nm to be excited to a Rydberg state,[56] photons at 184.9 nm can promote the radical to the Rydberg state while photons at 253.7 nm cannot. The electronically excited radical denoted by CH_3^* in Reactions 3 and 4 may

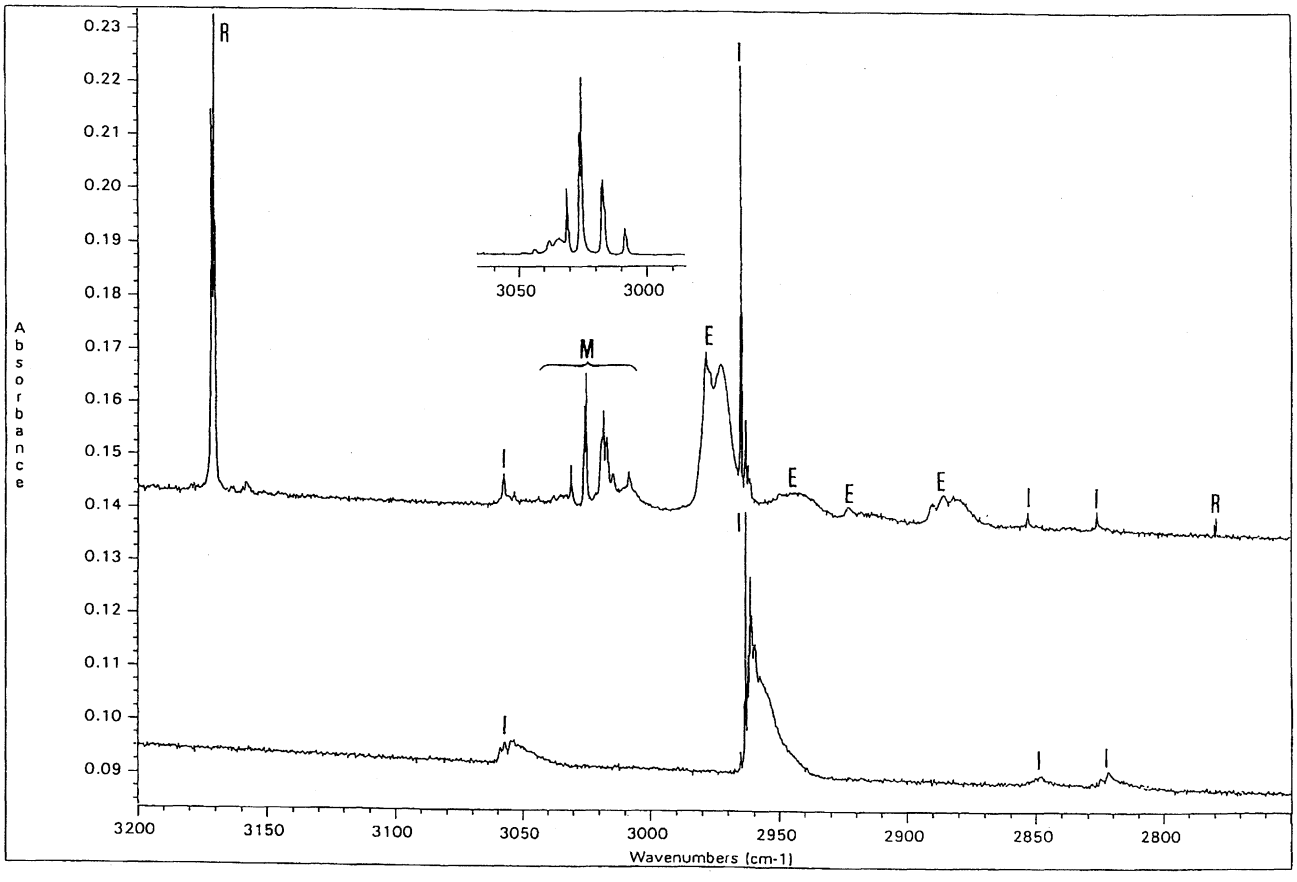

Fig. 9. FTIR spectra of methyl iodide in solid parahydrogen before (bottom) and after (top) irradiation by a low pressure mercury lamp.

react with surrounding hydrogen molecules to give methane (Reactions 3 and 4). 2) Photons at 253.7 nm dissociate the C–I bond of the iodide to yield kinetic methyl radical denoted by $CH_3^{\#}$ in Reaction 5 but the excess kinetic energy, that is, the difference between the impinging photon energy ($h\nu \cong 4.9$ eV) and the sum of the bond dissociation energy ($\cong 2.3$ eV) and the internal energy of the photofragments[57] is not utilized to promote the reaction between the kinetic methyl radical and hydrogen molecule (Reactions 5 and 6).

$$CH_3 + h\nu \text{ (184.9 nm, but not 253.7 nm)} \rightarrow CH_3^* + I, \quad (3)$$

$$CH_3^* + H_2 \rightarrow CH_4 + H, \quad (4)$$

$$CH_3I + h\nu(253.7 \text{ nm}) \rightarrow CH_3^{\#} + I, \quad (5)$$

$$CH_3^{\#} + H_2 \not\rightarrow CH_4 + H. \quad (6)$$

Since the activation energy of the thermal reaction between methyl radical and hydrogen molecule is reported at approximately 0.5 eV, which is much lower than the above excess energy,[58] the failure of the reaction by the 253.7 nm photon indicates that the kinetic methyl radical is quickly dissipated in solid parahydrogen. This may well be due to the fact that the thermal conductivity of solid parahydrogen is distinctly high as mentioned above.

A remarkable difference between the systems of CH_3I and CD_3I has recently been found.[59] While the ground state CH_3 radical does not react with hydrogen in the dark at 5 K, as stated above (Reaction 2), CD_3 radical does react under the same condition to form CD_3H (Reaction 7).

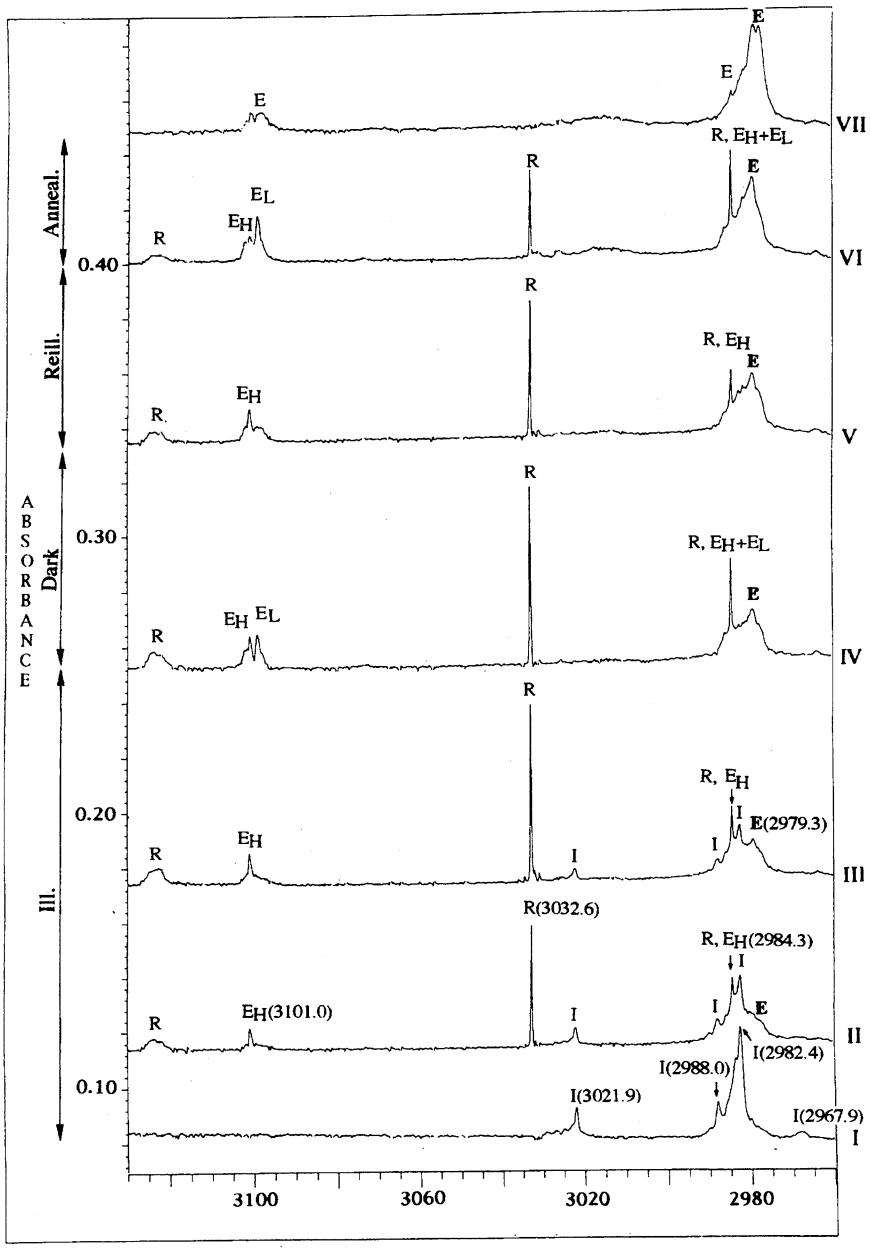

Fig. 10. FTIR spectra of ethyl iodide in solid parahydrogen. Spectra A—D demonstrate the effect of UV irradiation, E vs. D of standing under dark, and F vs. E of reirradiation.

$$CD_3 + H_2 \rightarrow CD_3H + H \quad \text{(at 5 K)}. \qquad (7)$$

This remarkable difference between Reactions 2 and 7 is most unusual, but the experimental evidence of spectral change is clear-cut and is attributed to the difference in the zero-point vibrational energy between CH_3 and CD_3 systems.[59]

The appearance of the absorption of ethane in Fig. 9 needs some consideration. First, the initial concentration of methyl iodide (approximately 0.01%) in the sample in Fig. 9 was relatively high enough to allow some of the iodide to form clusters. In fact, each iodide absorption peak shown in the lower panel of Fig. 9 is broadened by absorption extending toward lower frequencies, which is considered to be due to iodide clusters. On reducing the initial concentration of methyl iodide to, say, 0.003%, the formation of ethane is drastically reduced leaving only methyl radical and methane as the photolysis products.[44] This result suggests that the formation of ethane has something to do with cluster formation of methyl iodide in the sample before UV irradiation. One might conclude that two methyl radicals produced by the photolysis of two methyl iodides in clusters encounter each other and form ethane by recombination. However, since the absorption of methyl radical remains unchanged within the experimental time scale, such diffusive motion of the massive radical in the solid at 5 K is implausible. A hint to solve the question seems to be in the result of photolytic studies of methyl iodide in jet-cooled molecular beams.[60—62]

Syage and Steadman irradiated methyl iodide clusters $(CH_3I)_n$ with a picosecond laser pulse of 266 nm photons and analyzed the products by REMPI (resonance enhanced multiphoton ionization) combined with mass spectrometry.[60] They showed that the formation of I_2 and $I_2(CH_3I)_{n-2}$ within the cluster is completed in less than 10 picoseconds. Such a short time is incompatible with the ordinary two-step mechanism, $CH_3I \rightarrow CH_3 + I$ followed by $2I \rightarrow I_2$, under their experimental condition. Therefore, they considered that some new reaction peculiar to the cluster is involved.[60]

Similarly, Donaldson et al. found that irradiation of methyl iodide clusters in molecular beams by a nanosecond laser of 248 nm photons gives iodine molecules in the electronic ground state via a one-photon process and that the rotational temperature of the iodine molecule is significantly lower than room temperature.[60—62] In order to explain the result, they proposed a model of iodide dimer in which the two iodine atoms face each other and the dimer itself absorbs one photon to undergo a smooth concerted reaction, yielding a cold iodine molecule and ethane and/or two methyl radicals[62] (Reaction 8).

$$CH_3I \cdots ICH_3 + h\nu \rightarrow I_2 + 2C_2H_6 \text{ and/or } 2CH_3. \qquad (8)$$

Thus, in the experiment with approximately 0.01% CH_3I/p-H_2, some of the iodide are considered to be in the dimeric form, as shown in Reaction 8, and that the absorption of one photon by the dimer causes the formation of I_2 and ethane by a concerted reaction similar to that in the molecular beam.

Photolysis of Ethyl Iodide. On going from methyl to ethyl, photolytic reactions become more varied than expected from the result of the methyl iodide system.[52] The apparently complicated spectral changes, however, can be accounted for consistently because of the sufficient spectroscopic resolution.

If the reaction mechanism were completely analogous to that of methyl iodide, one would expect the formation of ethyl radical, ethane, and butane. Experimentally, however, butane is not formed at all, but two kinds of ethylene with slightly different transition frequencies are found.[52] This re-

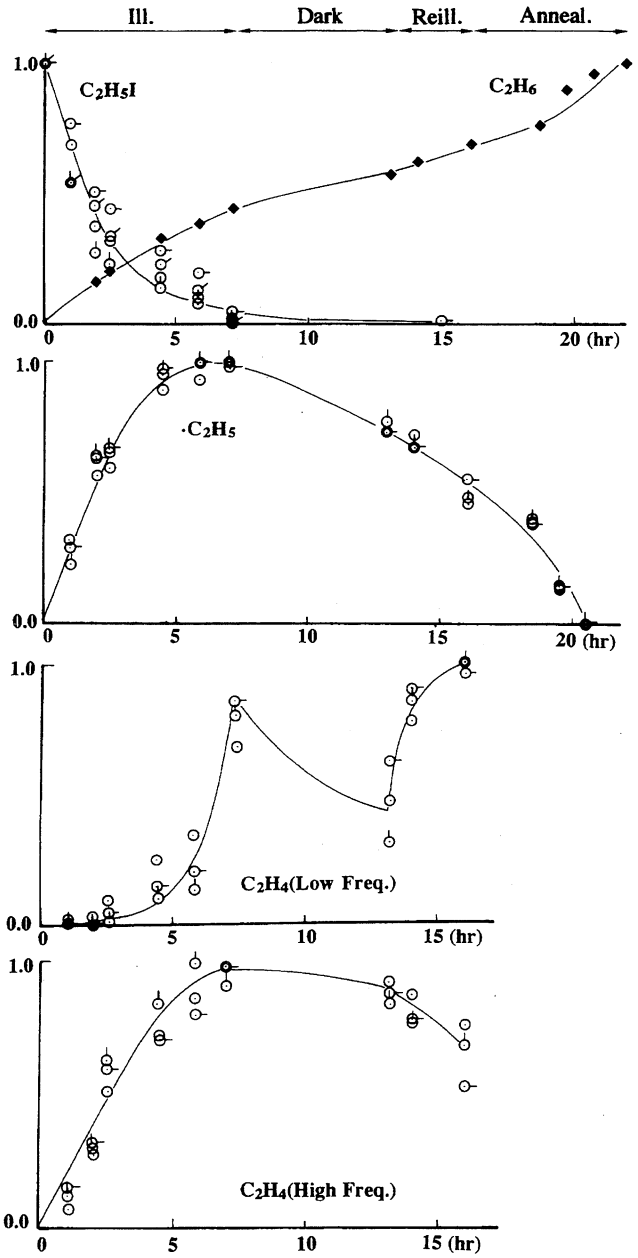

Fig. 11. Profile of the temporal change of ethyl iodide (top), ethyl radical (second), low-frequency ethylene (third), and high-frequency ethylene (bottom). Notations of Ill. Reill. and Anneal. atop the figure mean UV irradiation, reirradiation, and annealing, respectively. The sample was annealed at 6.0—9.0 K for five minutes and recooled to approximately 5.0 K before recording the spectra.

sult will be explained in the rest of this section.

Figure 10 demonstrates representative spectra before UV irradiation (A), after continual irradiation (B,C, D), after subsequent standing under dark at 5 K (E), and after reirradiation (F).[52] The symbols I, R, E, E_H, and E_L stand for ethyl iodide, ethyl radical, ethane, and the two kinds of ethylene associated with higher and lower transition frequencies.

Figure 11 shows temporal changes of the observed species. In the period of UV irradiation, ethyl iodide decays exponentially along with the appearance of ethyl radical. It happens by coincidence that ethyl radical absorbs 253.7 nm photons efficiently to be excited to a Rydberg state and yields ethylene by C–H bond dissociation in the methyl group of the radical.[63] Thus, we have the reaction schemes below.

$$C_2H_5I + h\nu \rightarrow C_2H_5 + I, \quad (9)$$

$$C_2H_5 + h\nu \rightarrow C_2H_4 + H. \quad (10)$$

Figure 10 reveals that the absorptions assigned to ethylene consist of two close-lying components designated as E_H and E_L, which are amplified in Fig. 12 for better legibility.

In Fig. 12 not only the spectral region in Fig. 10 but also two other regions of 1444—1438 and 964—942 cm^{-1}, where CH_2 scissoring and wagging modes of ethylene appear, are demonstrated. Among the three panels of Fig. 12, parallel behavior of the two kinds of ethylene is seen throughout the stages of the first irradiation, the following dark standing, and the reirradiation. Since the formation of ethylene via the photolysis of ethyl radical (Reaction 10) requires a second photon, its growth should be slow at the beginning of irradiation. Comparison of Figs. 11 and 12 indicates that E_L should be regarded as such ethylene. It should be noted that such ethylene produced by Reaction 10 must be near the iodine atom produced from the primary photolysis of ethyl iodide (Reaction 9). Since π electronic systems such as alkenes and aromatic hydrocarbons are known to form a charge-transfer complex with halogen atoms,[64] the low frequency ethylene is regarded as ethylene produced by Reaction 10 but is complexed with the iodine atom (Reaction 11).

$$C_2H_4 + I \rightarrow C_2H_4 \cdots I. \quad (11)$$

Contrary to the slowly appearing E_L the other ethylene, designated E_H, grows linearly with the irradiation time from the beginning. This apparently enigmatic behavior of E_H may be accounted for by noticing that the butane expected by analogy of Reaction 8 is absent. According to Donaldson et al.,[62] ethyl iodide dimers in jet-cooled molecular beams also are subjected to a concerted one-photon decomposition (Reaction 12) similar to that for methyl iodide dimers.

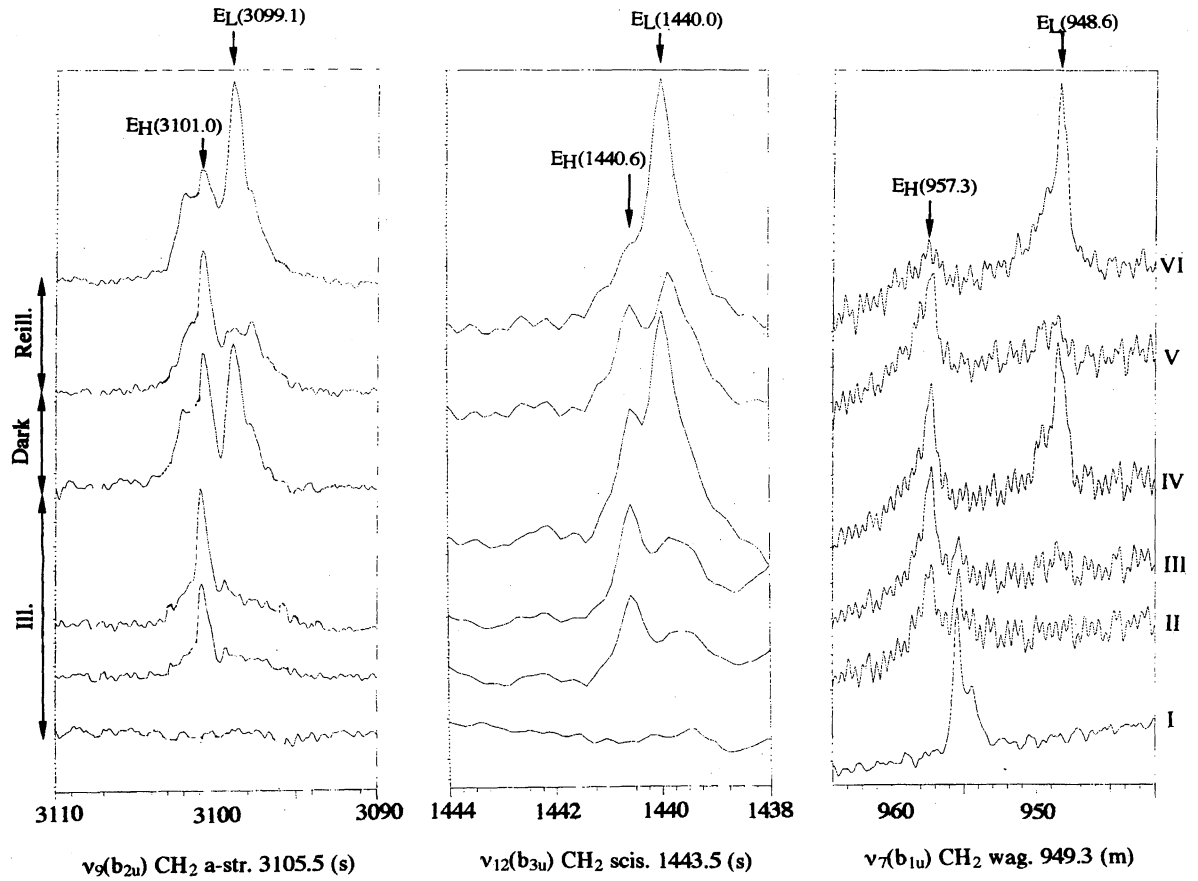

Fig. 12. FTIR spectra of ethylene in three regions, CH_2 asymmetric stretching (left), CH_2 scissoring (middle), and CH_2 wagging (right). E_H and E_L stand for high-frequency and low-frequency ethylene, respectively. The behavior of each ethylene is common to the three spectral regions throughout the seven stages of irradiation, standing under dark, and reirradiation.

$$C_2H_5I\cdots IC_2H_5 + h\nu \rightarrow I_2 + C_4H_{10} \text{ and/or } 2C_2H_5. \quad (12)$$

Therefore, if such reaction of the dimer takes place in the present experiment also, the hydrocarbon product in Reaction 12 has to be two ethyl radicals rather than butane which is not detected at all. The two close-lying radicals in Reaction12 may be subjected to the following disproportionation reaction via an H atom tunneling transfer.

$$C_2H_5 + C_2H_5 \rightarrow C_2H_4 + C_2H_6. \quad (13)$$

The reason why the two ethyl radicals in Reaction 12 prefer disproportionation to recombination to butane is not immediately clear. The massive radicals immobilized in the solid at 5 K may not be allowed to adjust themselves for recombination while the proposed H atom tunneling may proceed even if the radicals are immobile.

If the disproportionation follows immediately after Reaction 12, the ethylene formed by Reaction 13 grows linearly with the irradiation time, which is consistent with Fig. 11 if the ethylene in Reaction 13 is identified with E_H. Such ethylene should find a nearby iodine molecule produced by Reaction 12. The slightly higher frequencies of E_H than those of E_L are closer to the frequency of ethylene in the gas phase. This is reasonable because the degree of charge-transfer complexation of ethylene-iodine molecule should be weaker than that of ethylene-iodine atom assumed to correspond to E_L.[65]

Based on the above assumption of two kinds of ethylene, we have explained temporal changes shown in Figs. 10, 11, and 12 in all the stages.[52] Solid parahydrogen permits us to observe various subtle chemical reactions in cryogenic media on account of the absence of the preventive cage effect.

Conclusion

This Account has surveyed recent work dealing with solid parahydrogen which should be useful from the viewpoints of both high-resolution spectroscopy and photochemical study. So far, this work involves rotation-vibration spectroscopic studies. However, since solid parahydrogen is transparent up to vacuum UV region, extension of the study to electronic spectroscopy should provide detailed information on potential energy surface and various dynamics of electronically excited molecules in solid hydrogen. Chemical reactions at low temperatures have been less explored compared with those at higher temperatures. However, low temperature chemistry is becoming important in connection with new chemistry in jet-cooled molecular beams and stratosphere chemistry at subambient temperatures as well as molecular evolution in the interstellar space, in particular, on cold surfaces of grain dusts.[66,67] Sudies using solid parahydrogen as the new matrix will undoubtedly contribute to development of new frontiers in chemistry.

The authors are most grateful to Professors Eizi Hirota and Takeshi Oka for their interest in the present work. The work is mainly supported by the Grants-in-Aid for Scientific Research on Priority Areas (Free Radicals) from the Ministry of Education, Science, Sports and Culture.

References

1) E. Whittle, D. A. Dowes, and G. C. Pimentel, *J. Chem. Phys.*, **22**, 1943 (1954).
2) I. Norman and G. Porter, *Nature*, **174**, 508 (1954).
3) H. Broida and J. R. Pellam, *Phys. Rev.*, **95**, 845 (1954).
4) G. N. Lewis, D. Lipkin, and T. Magel, *J. Am. Chem. Soc.*, **63**, 3005 (1941).
5) M. E. Jacox, "Vibrational and Electronic Energy Levels of Polyatomic Transient Molecules," *J. Phys. Chem. Ref. Data*, Monograph 3 (1994); VEEL Version 5.0 to appear in *J. Phys. Chem. Ref. Data*.
6) V. E. Bondybey and V. A. Apkarian, *Chem. Phys.*, **189**, 137 (special issue) (1994).
7) M. Okumura, M.-C. Chan, and T. Oka, *Phys. Rev. Lett.*, **62**, 32 (1989).
8) T. Momose, D. P. Weliky, and T. Oka, *J. Mol. Spectrosc.*, **153**, 760 (1992).
9) D. P. Weliky, K. E. Kerr, T. J. Byers, T. Momose, Y. Zhang, and T. Oka, *J. Chem. Phys.*, **105**, 4461 (1996).
10) T. Oka, *Annu. Rev. Phys. Chem.*, **44**, 199 (1993).
11) T. Momose, *J. Chem. Phys.*, **107**, 7695 (1997).
12) T. Momose, M. Miki, T. Wakabayashi, T. Shida, M.-C. Chan, S. S. Lee, and T. Oka, *J. Chem. Phys.*, **107**, 7707 (1997).
13) T. Momose, H. Katsuki, H. Hoshina, N. Sogoshi, T. Wakabayashi, and T. Shida, *J. Chem. Phys.*, **107**, 7717 (1997).
14) T. Shida, E. Haselbach, and T. Bally, *Acc. Chem. Res.*, **17**, 180 (1984).
15) T. Shida, "Electronic Absorption Spectra of Radical Ions," Physical Sciences Data 34, Elsevier Science Publishers, Amsterdam (1988).
16) T. Shida, *Annu. Rev. Phys. Chem.*, **42**, 55 (1991).
17) T. Shida, in "Radical Ionic Systems," ed by A. Lund and M. Shiotani, Kluwer Academic Publishers, Dordrecht (1991), Chaps. I.7 and II.6.
18) T. Shida, T. Kato, and T. Momose, in "Dynamics of Excited Molecules," ed by K. Kuchitsu, Elsevier Science Publishers, Amsterdam (1994), Chap. 14.
19) T. Miyazaki, K. Yamamoto, and J. Arai, *Chem. Phys. Lett.*, **219**, 405 (1994).
20) M. E. Fajardo, S. Tam, T. L. Thompson, and M. E. Cordonnier, *Chem. Phys.*, **189**, 351 (1994).
21) M. W. Windsor, in "Formation and Trapping of Free Radicals," ed by A. M. Bass and H. P. Broida, Academic Press, New York (1960), Chap. 13, p. 387—409.
22) W. Kolos and L. Wolniewicz, *J. Chem. Phys.*, **45**, 509 (1966); **49**, 404 (1968).
23) I. F. Silvera, *Rev. Mod. Phys.*, **52**, 393 (1980).
24) L. H. Nosanow, *Phys. Rev.*, **146**, 120 (1966).
25) P. C. Souers, "Hydrogen Properties for Fusion Energy," University of California Press, Berkeley (1986).
26) T. Momose, T. Wakabayashi, and T. Shida, *J. Opt. Soc. Am*, **B13**, 1706 (1996).
27) H. Adams, J. L. Hall, R. F. Curl, J. V. V. Kasper, and F. K. Tittel, *J. Opt. Soc. Am.*, **B1**, 710 (1996).
28) L. Pauling, *Phys. Rev.*, **36**, 430 (1930).
29) A. Cabana, G. B. Savitsky, and D. F. Horning, *J. Chem. Phys.*, **39**, 2942 (1963).
30) A. Chamberland , R. Belzile, and A. Cabana, *Can. J. Chem.*, **48**, 1129 (1970).
31) F. H. Frayer and G. E. Ewin, *J. Chem. Phys.*, **48**, 781 (1968).

32) B. Nelander, *J. Chem. Phys.*, **82**, 5340 (1985).
33) L. H. Jones, S. A. Ekberg, and B. I. Swanson, *J. Chem. Phys.*, **85**, 3203 (1986).
34) L. H. Jones and S. A. Ekberg, *J. Chem. Phys.*, **87**, 4368 (1987).
35) M. Hepp, G. Winnewisser, and K. M. T. Yamada, *J. Mol. Spectrosc.*, **164**, 311 (1994).
36) R. E. Miller and J. C. Decius, *J. Chem. Phys.*, **59**, 4871 (1973).
37) J. T. Hougen, "International Review of Science, Physical Chemistry, Ser. 2, Vol. 3, Spectroscopy," ed by D. A. Ramsay, Butterworth, London (1976).
38) For example: M. Tinkham, "Group Theory and Quantum Mechanics," McGraw Hill, New York (1964).
39) For example: G. Herzberg, "Molecular Spectra and Molecular Structure, Vol. II, Infrared and Raman Spectra of Polyatomic Molecules," Krieger Publishing Co., Malabar, Florida (1991).
40) T. Amano, P. F. Bernath, C. Yamada, Y. Endo, and E. Hirota, *J. Chem. Phys.*, **77**, 5284 (1982).
41) A. Snelson, *J. Phys. Chem.*, **74**, 537 (1970).
42) J. Pacansky and J. Bargon, *J. Am. Chem. Soc.*, **97**, 6896 (1975).
43) M. E. Jacox, *J. Mol. Spectrosc.*, **66**, 272 (1977).
44) T. Momose, M. Miki, M. Uchida, T. Shimizu, I. Yoshizawa, and T. Shida, *J. Chem. Phys.*, **103**, 1400 (1995).
45) M. Miki, T. Wakabayashi, T. Momose, and T. Shida, *J. Phys. Chem.*, **100**, 12135 (1996).
46) S. Tam, M. Macler, and M. E. Fajardo, *J. Chem. Phys.*, **106**, 8955 (1997).
47) I. L. Mador, *J. Chem. Phys.*, **22**, 1617 (1954).
48) G. C. Pimentel, "Formation and Trapping of Free Radicals," ed by A. M. Bass and H. P. Broida, Academic Press, New York (1960), Chap. 4, pp. 69—115.
49) L. Andrews and G. C. Pimentel, *J. Chem. Phys.*,**47**, 3637 (1967).
50) L. E. Brus and V. E. Bondybey, *J. Chem. Phys.*, **65**, 71 (1976).
51) T. Momose, M. Uchida, N. Sogoshi, M. Miki, S. Masuda, and T. Shida, *Chem. Phys. Lett.*, **246**, 583 (1995).
52) N. Sogoshi, T. Wakabayashi, T. Momose, and T. Shida, *J. Phys. Chem.*, **101A**, 522 (1997).
53) N. Sogoshi, T. Wakabayashi, T. Momose, and T. Shida, unpublished.
54) D. N. Batchelder, "Rare Gas Solids," ed by M. L. Klein and J. A. Venables, Academic Press, London (1977), Vol. II, Chap. 14, pp. 883—819.
55) M. Fushitani, T. Momose, and T. Shida, to be published.
56) G. Herzberg, "Molecular Spectra and Molecular Structure, Vol.III, Electronic Spectra and Electronic Structure of Polyatomic Molecules," Krieger Publishing Co., Malabar, Florida (1991).
57) T. Suzuki, H. Kanamori, and E. Hirota, *J. Chem. Phys.*, **94**, 6607 (1991).
58) E. Kraka, J. Gauss, and D. Cremer, *J. Chem. Phys.*, **99**, 5306 (1993), and references therein.
59) T. Momose, N. Sogoshi, H. Hoshina, H. Katsuki, T. Wakabayashi, and T. Shida, to be published.
60) J. A. Syage and J. Steadman, *Chem. Phys. Lett.*, **166**, 159 (1990).
61) Y. B. Fan and D. J. Donaldson, *J. Phys. Chem.*, **96**, 19 (1992).
62) Y. B. Fan, K. L. Randall, and D. J. Donaldson, *J. Chem. Phys.*, **98**, 4700 (1993).
63) J. L. Brum, S. Deshmukh, and B. Koplitz, *J. Chem. Phys.*, **95**, 2200 (1991).
64) S. J. Rand and R. L. Strong, *J. Am. Chem. Soc.*, **82**, 5 (1960).
65) R. S. Mulliken and W. B. Person, "Molecular Complexes," Wiley-Interscience, New York (1969).
66) E. Herbst, *Annu. Rev. Phys. Chem.*, **46**, 27 (1995).
67) I. R. Sims and I. W. M. Smith, *Annu. Rev. Phys. Chem.*, **46**, 109 (1995).

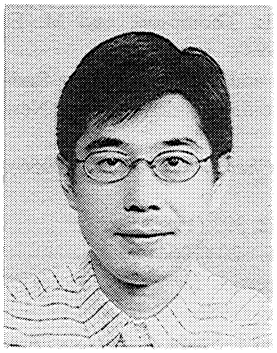

Takamasa Momose was born in 1962 in Matsumoto. He received his B.S. in 1984 and his M.S. in 1986. In 1987 he was appointed as assistant professor at Kyoto University. He was awarded his PhD. in 1991 from Kyoto University. He worked as a postdoctoral fellow for Professor Takeshi Oka at The University of Chicago from 1991 to 1993. In 1995 he was promoted to associate professor of physical chemistry in The Graduate School of Science at Kyoto University. His scientific interest ranges from quantum chemistry, high-resolution molecular spectroscopy, and low-temperature physics of condensed matter. He received The Chemical Society of Japan Award for Young Chemists for 1995.

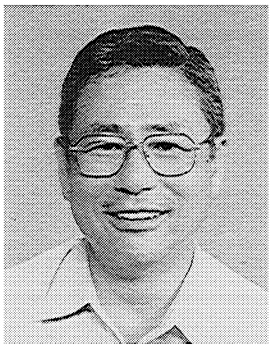

Tadamasa Shida received his B.S. in 1958, his M.S. in 1961, and his Ph D. in 1964, all in chemistry from The University of Tokyo. He worked at The Institute of Physical and Chemical Research from 1958 to 1974 until he joined The Faculty of Science, Kyoto University as associate professor. He was promoted to professor of chemistry in 1983 and was reappointed in 1995 to Professor of Physical Chemistry at The Graduate School of Science, Kyoto University. His scientific interests lie in molecular spectroscopy of transient molecules and the chemical reaction mechanism. He authored the book "Electronic Absorption Spectra of Radical Ions", Elsevier, 1988.